

APPLICATIONS OF A NONLINEAR DYNAMICS TOOL TO ROTORCRAFT DESIGN PROBLEMS AT BELL HELICOPTER TEXTRON INC.

Ashish K. Sareen
Principal Engineer

Michael R. Smith
Principal Engineer

B. Robert Mullins
Staff Engineer

Bell Helicopter Textron, Inc., Fort Worth, Texas

Abstract

This paper addresses application of a nonlinear transient dynamics tool to a number of important aircraft design problems at Bell Helicopter Textron Inc. involving a high degree of material and geometric nonlinearity, with some problems involving fluid-structure interaction. Specifically, applications to design problems such as helicopter skid gear dynamic drops, rotorcraft impact on ground and calm water, ballistic penetration of composite fuel-filled wing tanks, bird-strike analysis of airframe structures, and subfloor crushing during impact are studied using a commercially available code, MSC/DYTRAN. For each of these problems, the analysis data are compared with the available test data. With the goal of developing predictive analytical methodologies using the design support tool, these applications provide an understanding of modeling parameters and techniques that dictate successful correlation with the test data.

Introduction

Bell Helicopter Textron Inc. has been involved in nonlinear dynamics and crashworthiness analysis development for a number of years. Bell has a comprehensive system of advanced nonlinear dynamics and crash impact analysis tools that provide rapid and reliable analysis of critical airframe components, such as the fuselage, landing gear, and seats. Among others, these analytical tools include KRASH, SOMLA, LS-DYNA, and MSC/DYTRAN™*.

In this paper, specific applications of a nonlinear dynamics tool have focused on evaluating the suitability of the MSC/DYTRAN tool by performing analysis-test correlation on a number of problems. Problems utilizing MSC/DYTRAN have included the following:

1. Reserve energy dynamic drop analysis to compute attachment fitting loads and evaluate the energy-absorption behavior for skid gears during dynamic impacts in level, roll, run-on,

and level landings with sideward obstruction (Refs. 1 and 2).

2. Hydraulic ram simulations of a high-speed projectile penetrating through a fluid-filled tank. Computed results agree closely with measured projectile tumbling and peak overpressures in the fluid. Successful dynamic simulation of hydraulic ram may alleviate some future design support testing requirements (Refs. 3 and 4).
3. Hydraulic ram ballistic analysis of simulated outboard wing fuel bay on the tiltrotor aircraft to demonstrate the relative performance of bonded rib-to-skin attachment designs in surviving ram from a ballistic impact. MSC/DYTRAN simulations involve armor-piercing projectile impact on a composite wing structure with integral fuel tanks (Refs. 3 and 4).
4. Analyses of a single-cruciform thermoplastic energy-absorbing subfloor structure to simulate the progressive crushing when dropped at 30 ft/s (9 m/s). Crush distance and deceleration time histories were compared with measured test data and available DYNA3D results. The effort provided better understanding of modeling the thermoplastic composite failure mechanisms (Refs. 5 and 6).
5. Airframe response simulations during water ditching. MSC/DYTRAN analyses of airframe impacts on water helped develop the capability of predicting accelerations and fluid pressures acting on the aircraft structure. Parameters affecting airframe response such as fluid mesh density, Lagrangian/Eulerian fluid formulations, and use of flow boundaries led to a better understanding of structural behavior and surface pressures during water ditching (Refs. 7 and 8).
6. Bird-strike tolerance of the BA609 wing and horizontal stabilizer leading edge and overwing fairing to the impact of a 4-lb (1.8-kg) bird at 240 knots (444.5 km/h). Using data for bird-strike tests performed at Cessna, excellent correlation was observed for wing leading edge configurations. As a weight reduction measure, several metallic and composite configurations were subsequently analyzed using an Eulerian bird model.

* MSC/DYTRAN is a trademark of MSC Software.

7. Analyze the effectiveness of MSC/DYTRAN for simulating helicopter ground impacts in which fuel tanks are surrounded by structure. This effort involved the analysis model development of the advanced lightweight rotorcraft (ALR) fuselage center section to correlate the analytical impact pressures and structural response with the ALR center-section drop test data.

Following a description of the nonlinear dynamics tool, some of these problems are described below in detail.

Description of MSC/DYTRAN Analysis Tool

MSC/DYTRAN is a general-purpose finite-element code that uses the explicit formulation of the finite-element method to treat problems with geometric and material nonlinearity. It contains both Lagrangian and Eulerian processors. The Lagrangian processor uses a control mass approach and is primarily applicable to structural problems. The Eulerian processor uses a control volume approach and is used mainly for fluid problems. The two processors can be coupled in two different ways (ALE and general coupling), depending on the nature of the problem.

The MSC/DYTRAN structural model can be composed of isotropic beam, shell, and solid, or orthotropic shell elements with appropriate yield and failure criteria. For structural problems involving impacts or crushing, a single surface or surface-to-surface contact is available. It is possible in MSC/DYTRAN to model the structure as a Lagrangian mesh and have it surrounded by the fluid modeled either as Eulerian or Lagrangian solid elements having no yield strength. Depending on the objectives of the model, each approach contains advantages and disadvantages. Thus, as with any predictive methodology, the user understanding of the code's modeling parameters and techniques is essential in achieving a successful analysis-test correlation. Description of other features of the code is included in application to the specific problems described below.

Skid Gear Dynamic Drop Analysis

The first design problem analyzes the structural behavior of helicopter skid gear during a reserve-energy landing. Helicopter skid gear must provide sufficient strength to survive several thousand landings while providing adequate energy absorption for hard landings. The analysis method employs MSC/DYTRAN to simulate the landing gear dynamic drop on an impact surface with an

unrestricted definition of skid gear geometry and the impact condition. In accordance with the revised AR-56 aeronautical requirement criteria (Ref. 9), the method allows analysis of level landings, one-skid landings with rolled attitudes, landing-with-drag, and level landings with lateral obstructions. The following paragraphs describe the test correlation of the full-scale reserve energy landing-with-drag analysis of the Model 407 helicopter skid gear. Calibration of attachment fitting level landing loads, one-skid landing analysis in rolled attitude, and associated methodology details for level and rolled landing impacts are available in Refs. 1 and 2.

Prior to the development of MSC/DYTRAN-based methodology, the analytical tools used to support design of helicopter skid gear were restricted to level landings; they incorporated empiricism, and did not include full definition of skid gear geometry or skid-to-ground interaction.

For dynamic drop simulation of the Model 407 helicopter skid gear landing-with-drag, the helicopter was modeled as a rigid body fuselage model with detailed definition of skid gear. The mass and inertia of the fuselage are lumped at its effective cg location and connected to the top of the gear attachment fittings (Fig. 1). The attachment fittings connecting the fuselage to the skid gear are modeled as stiff elastic springs. The gear cross tube and skid tubes are modeled using beam elements with a piecewise linear elastoplastic material definition including the yield and plastic strain failure criteria.

The impact surface is modeled as a rigid panel with constraints on its translational and rotational motion. Interaction of skid gear with the impact surface, modeled using a grid-to-surface contact, allows the forces of the dynamic drop to be transmitted. Static and kinetic friction coefficients are used to define sliding contact of the skid tubes on the impact surface. Friction coefficients can be varied to represent skid gear contact with different impact surfaces, viz., concrete, hangar floor, or icy surface.

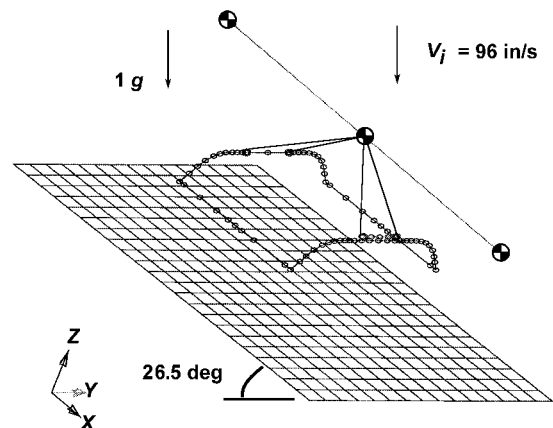


Fig. 1. MSC/DYTRAN model for M407 landing-with-drag.

The friction coefficient, μ , is defined in MSC/DYTRAN as follows:

$$\mu = F_k + (F_s - F_k) e^{-\beta v} \quad (1)$$

where F_k is the kinetic friction coefficient, F_s is the static friction coefficient, β is the exponential decay coefficient, and v is the relative velocity between the sliding components.

A landing-with-drag drop test of a production skid gear was conducted to provide data for verification of a corresponding MSC/DYTRAN analysis. The drop test specimen consisted of a production Model 407 skid gear assembly fixed beneath a welded-steel structure that simulated the helicopter. The fixture assembly, weighing 3,050 lb (1,383.5 kg), was dropped onto a steel-plated ramp that was at an angle of 26.5 deg to the horizontal plane (Fig. 2). The skid tubes were aligned parallel with the ramped impact surface and positioned with a perpendicular distance of 10.74 inches (0.273 m) from the inclined surface. This allowed the drop fixture to fall a distance of 12.0 inches (0.305 m) and to reach an impact velocity of 8.0 ft/s (2.44 m/s) prior to skid tube contact. The corresponding velocity components in “aircraft” coordinates were 86.14 in/s (2.188 m/s) in the downward direction and 42.95 in/s (1.09 m/s) in the forward direction.

The inertial properties of the MSC/DYTRAN fixture model (Fig. 1) were adjusted to closely match the measured hardware weight and pitch inertia. The analysis used a static coefficient of friction of 0.5 (tungsten carbide on steel), a kinetic coefficient of 0.38, and an exponential decay coefficient of 0.1, based on laboratory tests. The MSC/DYTRAN skid gear assembly was positioned 0.10 inch (0.254 cm) above the rigid impact surface (measured

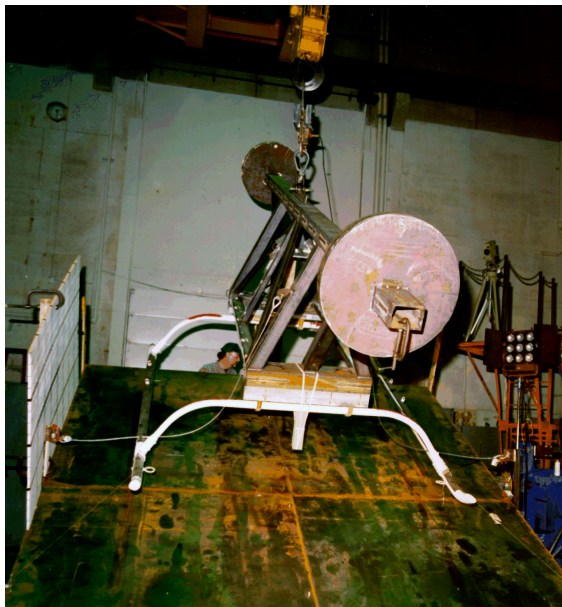


Fig. 2. Model 407 skid gear drop test setup.

perpendicularly). The resultant gravity vector was aligned 26.5 deg relative to the impact surface normal. An initial velocity was imparted to the analytical model in such a manner that its impact velocity corresponded with the drop test fixture.

The maximum vertical deflection of the cross tubes measured during the test was 9.0 inches (22.86 cm), as determined by high-speed film. The MSC/DYTRAN displacement time history, shown in Fig. 3, indicates the maximum forward and aft cross-tube deflection was 9.05 inches (22.98 cm) and 8.37 inches (21.26 cm), respectively. The time at which the test drop fixture was released was used as the start time ($t_0 = 0.0$ s). The analysis time data was translated to match the corresponding time of impact ($t_i = 0.21$ s).

Figs. 4 through 6 indicate that the analytical vertical acceleration pulses agree reasonably well with measured data in terms of pulse shape, duration, and peak response. All test and analysis acceleration data were low-pass filtered to eliminate fixture ringing from lower frequency structural modes.

The longitudinal acceleration, shown in Fig. 7, also shows reasonable fidelity with respect to the measured peak response, but not in duration. The integrated area under the longitudinal acceleration pulse indicates that the fuselage fixture lost more

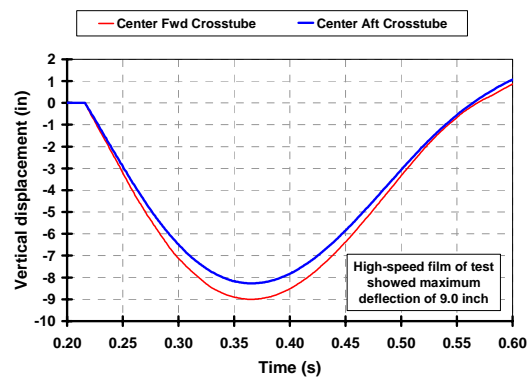


Fig. 3. Vertical displacement for landing-with-drag.

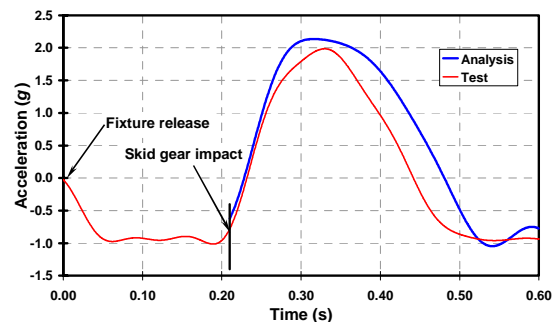


Fig. 4. Vertical acceleration at cg for landing-with-drag.

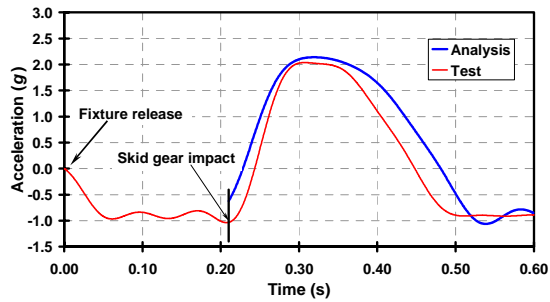


Fig. 5. Forward fitting vertical acceleration for landing-with-drag.

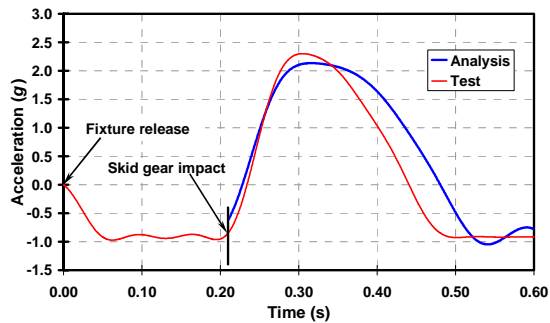


Fig. 6. Aft fitting vertical acceleration for landing-with-drag.

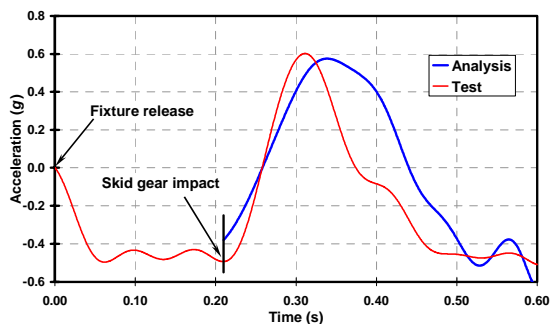


Fig. 7. Forward fitting longitudinal acceleration for landing-with-drag.

longitudinal velocity in the analysis than in test (In Fig. 7, note the larger area under the analytical pulse). This may be due to the fact that MSC/DYTRAN does not provide a means of representing directional friction. Longitudinally running weld-beads run the length of the lower surface of skid tubes, providing potentially different lateral and longitudinal friction.

Nevertheless, the peak calculated accelerations, both vertically and longitudinally, correlate closely with measured data. Since attachment-fitting loads are proportional with accelerations, it can be assumed that the calculated peak loads at the fittings would also correlate closely.

Thus, the MSC/DYTRAN analysis correlated well with the available drop test data for reserve energy landing-with-drag. Together with Ref. 1 and 2, the method validates MSC/DYTRAN as a design support tool for analyzing helicopter impacts in any attitude by quantifying the structural behavior. This significantly enhances the state-of-the-art in reserve-energy impact analysis to meet revised AR-56 criteria.

Ballistic Dynamics of Generic and Composite Wing Fuel Tank

The next design problem addresses wing ballistic design issues through analytical hydraulic ram simulations and correlation using an MSC/DYTRAN model of a high-speed projectile penetrating through a wing fuel tank. The hydraulic ram effects are a major combat threat to military aircraft. Penetration of bullets and other high-speed projectiles through fuel tanks generates intense pressure waves that can cause catastrophic failure of the fuel cell walls. This section highlights the potential of ballistic dynamics analysis to accurately simulate the multidisciplinary fluid-structure interaction, leading to better ballistic-survivable wing designs and thus to alleviate expensive qualification testing.

Penetration of a 12.7-mm armor-piercing incendiary (API) bullet into a generic water-filled tank is analyzed as a means to verify hydraulic ram pressures and projectile tumbling behavior. The generic tank hydraulic ram analysis paves the way for positioning the line-of-shot to ensure projectile impact at a pre-designated location and attendant failure analysis for a composite wing fuel tank using MSC/DYTRAN.

Accurate simulation of structural damage requires accurate modeling of the energy transfer from the projectile to the fluid and structure. This requires accurate simulation of projectile kinetics and kinematics, which in turn requires accurate simulation of fluid dynamics as well as fluid-structure interactive dynamics. All three phases of hydraulic ram, kinetic impulse, drag, and cavitation, were successfully simulated with MSC/DYTRAN. Inclusion of all of these phases in the analysis is important to accurately simulate projectile tumbling within the fluid. The analysis herein simulated the projectile penetration of the entry panel, the production of shock waves in the water, pressure drag on the projectile, and formation of a cavity region behind the bullet. Accurate simulation of hydraulic ram including failure mode prediction can be useful as a design tool to enhance ballistic tolerance as well as guiding pretest line-of-shot setup to ensure projectile strike and exit at critical locations.

Phases of Hydraulic Ram

There are three primary sequential phases in hydraulic ram: the shock (kinetic impulse) phase, the drag phase, and the cavitation phase.

Shock Phase. The kinetic impulse or shock phase occurs when the projectile initially penetrates the tank wall and impacts the fluid, producing a hemispherical shock wave. This shock wave propagates at sonic velocity through the fluid away from the projectile–fluid impact point, producing an impulsive load that acts on the entire surrounding tank wall. This impulse is most destructive close to its point of origin—near the entry hole.

Drag Phase. The projectile is slowed by viscous drag forces as it moves through the fluid. The resulting momentum transfer from the projectile to the fluid increases its kinetic energy, producing a pressure wave with lower intensity than in the shock phase, but with longer duration.

Cavitation Phase. As the projectile moves through the fluid, the fluid is displaced both along the axis of travel and radially to this axis. The radial velocity away from the projectile causes a wake to form at the aft end of the projectile. Behind this wake, a cavity forms where the pressure is below the vapor pressure of the fluid. As this cavity collapses, significant pressure pulses are generated that propagate through the fluid, causing the greatest damage to the opposing wall of the fuel tank, near the exit hole.

Projectile Tumbling

Projectile kinematics contributes significantly to the hydraulic ram effect. If the projectile tumbles in the fluid, the energy transferred from the projectile to the fluid during the drag phase is dramatically increased and the attendant structural loading is correspondingly increased. In addition, a tumbled projectile produces greater cavitation, which in turn produces greater pressure pulses. Pressure waves generated by a projectile in a fully tumbled attitude will be approximately five times more intense than those generated by the same projectile in its normal 0-deg yaw attitude. As

shown in Fig. 8, the projectile continues to tumble beyond the 90-deg yaw attitude along its trajectory before assuming a stable attitude.

Ballistic Modeling using MSC/DYTRAN

The MSC/DYTRAN models for ballistic simulations used both Lagrangian and Eulerian processors. The projectile and tank were modeled using Lagrangian shell elements while the fluid was modeled using Eulerian solid elements. The interaction between the generic/composite wing tank and projectile was modeled using structure-to-structure contact with friction.

Adaptive contact was used to transmit forces between the projectile and the tank. Adaptive contact allows a penetrating object to go through a closed surface after elements in its path have failed.

To transfer the fluid–structure interaction forces, the Lagrangian and Eulerian meshes are coupled using both Arbitrary-Lagrange–Euler (ALE) coupling and “General” coupling. ALE coupling is used between the tank wall and the fluid, which allows the fluid Eulerian mesh to follow the motion of the Lagrangian mesh as the tank wall deflects.

General coupling is used between the projectile and the fluid. General coupling allows arbitrary motion of the Lagrangian structure through the fixed Eulerian mesh. The Lagrangian structure forms a continuously moving flow boundary for the Eulerian fluid while the fluid simultaneously acts as a pressure load on the Lagrangian structure. The general coupling algorithm computes the volume fractions of the intersected Euler elements occupied by Lagrangian structure, and applies pressure forces to each intersected Euler element to displace the required amount of fluid out of the element. In contrast with ALE coupling, this approach allows unlimited deformation or movement of the Lagrange structure (necessary in the case of a penetrating projectile); but general coupling also requires a large number of CPU-intensive 3-D intersection calculations at every time step.

An initial penetration of the projectile into the Euler mesh at time step zero is necessary for general coupling to work properly. The general coupling

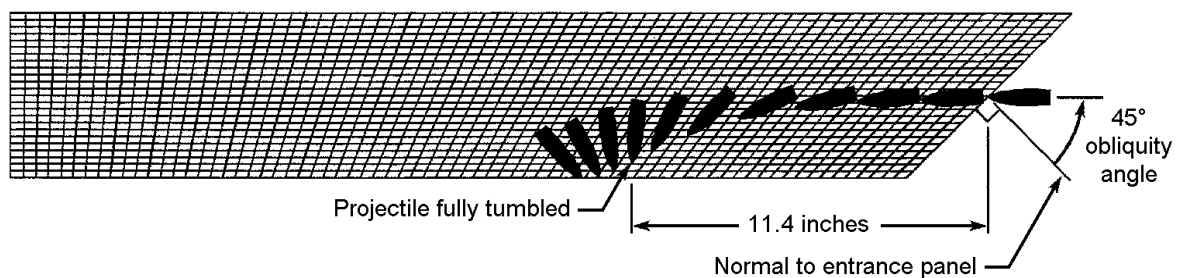


Fig. 8. Tumbling behavior for projectile penetrating at 45-deg obliquity.

algorithm only checks for penetrated or intersected Euler elements immediately adjacent to those already penetrated. Thus if elements are not initially penetrated, none will be found throughout the entire solution sequence.

In order to assess correlation with ballistic test data, two different tanks were modeled: a generic tank and a composite wing tank. Projectile tumbling and fluid pressures were correlated with the generic tank, while projectile trajectory and structural response and damage were correlated with the composite wing tank.

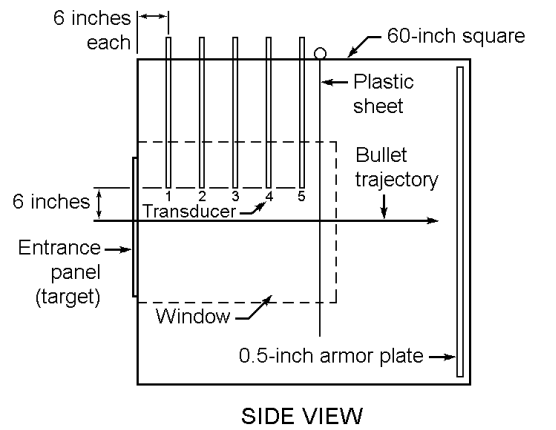
Generic Tank Test and Analysis Results

In the early 1970s, ballistic tests were conducted by the U.S. Naval Weapons Center (NWC) on a 60-inch (1.52-m) cube test cell. The water-filled, open-top test cell (Fig. 9) was shot with 12.7 mm API (armor-piercing incendiary) rounds at three different obliquity angles: 0 deg, 30 deg, and 45 deg. Five pressure transducers were positioned in the fluid along the line of shot to measure the pressure time histories. The pressure transducers were placed 6 inches (0.152 m) above the expected trajectory along 6-inch (0.152-m) intervals. Coordinates of the pressure transducers with respect to the test cell are listed in Fig. 9. High-speed motion picture data was taken to determine the projectile tumbling behavior.

The test cell walls were constructed of 1/8-inch-thick (3.2-mm) steel plates with angle iron reinforcements at the edges and an open top. A 1/2-inch (12.7-mm) steel plate at the rear wall prevented projectile exit from the cell. A 2- x 2-ft (0.61- x 0.61-m) entrance panel made of 0.063-inch-thick aluminum was held in place by compression between two rubber gaskets around the edges. Two 1-inch-thick (25.4-mm) plexiglass windows were placed on opposite sides of the cell to allow for high-speed photography.

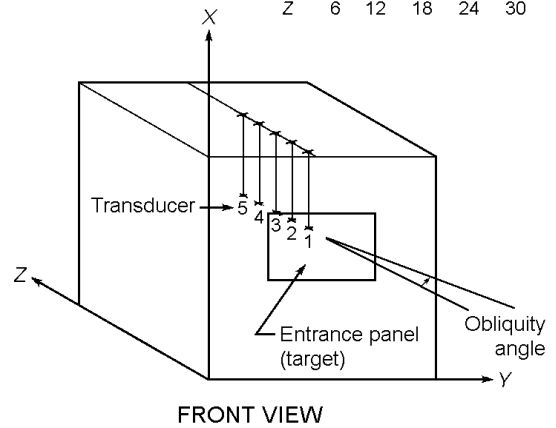
The generic tank analysis model has 92,160 Eulerian fluid elements. The properties of the water assume no viscosity and are determined from its mass and bulk modulus. To allow finer meshing along the shotline, the back 24 inches (0.61 m) of the tank are not explicitly modeled but are represented by a FLOW boundary. The FLOW boundary does not reflect pressure waves; rather, it simulates the presence of additional fluid beyond the mesh boundary. The tank model is 60 inches deep, 60 inches wide, and 36 inches long along the shotline (1.52 m x 1.52 m x 0.76 m).

The Euler mesh shown in Fig. 10 is composed of two distinct regions: a central "core" region, and the surrounding region extending to the tank wall. The core is sized and meshed for each obliquity angle so that the projectile stays within this finely meshed region throughout the analysis. The core



SIDE VIEW

Axis	Distance along axis, inches				
	1	2	3	4	5
X	36	36	36	36	36
Y	30	30	30	30	30
Z	6	12	18	24	30



FRONT VIEW

Fig. 9. Test Tank: side view and front view.

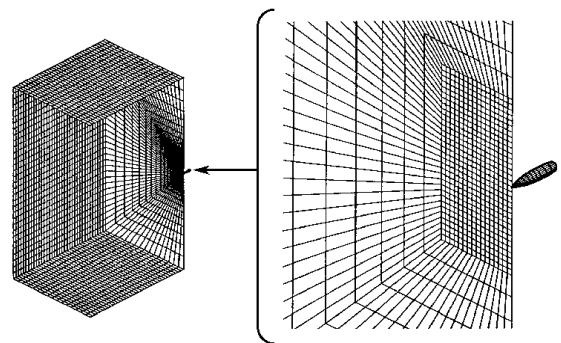


Fig. 10. Comparison of mesh densities of the projectile and the tank.

region is 8 inches wide by 8 inches deep, and extends 36 inches along the length of the tank (0.20 m x 0.20 m x 0.76 m). The core has a fine but constant mesh density with 36,864 elements. This mesh density yields good results at small projectile angles (i.e., when there is no tumbling), but some problems occur at high yaw angles, because it is possible for the projectile to become completely contained in one row of elements. Since MSC/DYTRAN uses first-

order approximations, the pressure within each element is assumed to be uniform. Thus when the projectile is fully contained in one row of elements, it experiences no pressure gradient along its trajectory vector and therefore no drag force opposing its motion. When the projectile moves into the next row of elements, it experiences a sudden pressure gradient. This causes multiple small pressure waves to be generated, which results in oscillations in the projectile deceleration (Fig. 11).

The tank walls in Fig. 10 are modeled with 7,168 Lagrangian shell elements representing the 1/8-inch-thick (3.2-mm) steel plate. The open top is modeled with elements having effectively no stiffness (thickness of 0.0001 inch [0.00254 mm]) and a density equal to water. The 12.7-mm projectile is modeled with 312 Lagrangian shell elements. These elements define the shape of the projectile, which is then specified as rigid with a RIGID card in the model.

The kinetic energy lost by the projectile as it penetrates the generic tank at 0-deg obliquity and travels through the fluid is shown in Fig. 11. During the first phase of hydraulic ram (initial impact and wall penetration), 3.3% of the total projectile kinetic energy is lost. Over the next 1.0 millisecond, the kinetic energy of the projectile is reduced to approximately 45% of its initial impact state. The evident oscillations in the projectile velocity between 0.6 and 0.8 millisecond are a result of the projectile being contained in one row of elements, and indicate that the projectile is in a nearly fully-tumbled state. The calculated distance for the projectile to reach a fully tumbled state is 18.97 inches (0.4818 m), which is within 14.0% of the measured distance of 17.00 inches (0.4318 m).

The shape of the calculated pressure contours in the fluid is visible in Fig. 12. The calculated peak overpressures in the fluid at the five transducer locations correlate within approximately 5% of the measured data, as indicated in Fig. 13. Other line-of-shot obliquity angles of 30 and 45 deg are presented in Refs. 3 and 4.

Correlation of results from the generic tank indicates that MSC/DYTRAN can accurately simulate the observed projectile trajectory and shows promise in accurately simulating hydraulic ram pressures.

Composite Wing Tank Ballistic Test and Analysis

The composite wing structure (Fig. 14) is composed of bonded rib-to-skin attachment with cocured stringer and spar caps made of bundled pultruded carbon epoxy rods to provide superior stiffness along the length of composite wing skin. While these mostly-bonded wing structures have the potential of cost and weight savings, their implementation

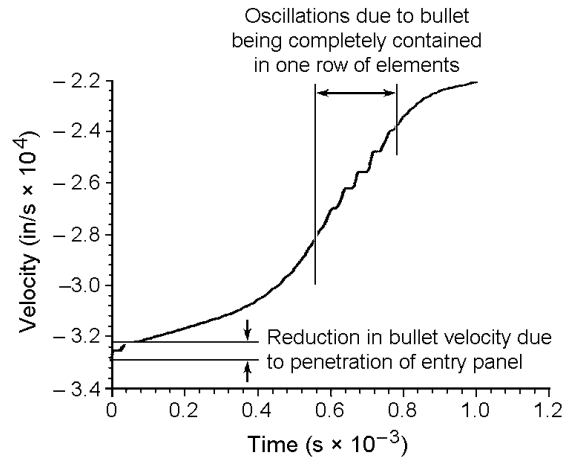


Fig. 11. Projectile velocity time history through generic tank.

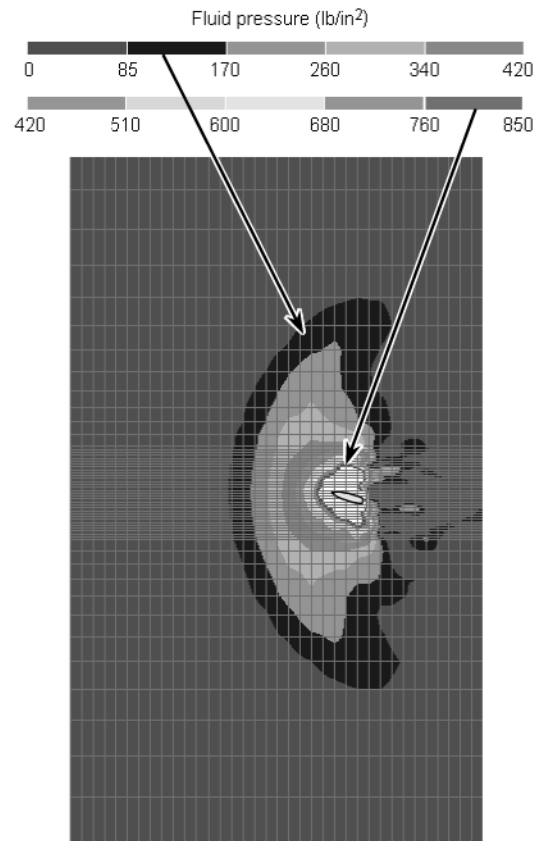


Fig. 12. Pressure contours for a partially tumbled projectile.

into future military aircraft is contingent on their suitability to provide the necessary structural integrity in surviving hydraulic ram. Accordingly, ballistic testing was required to demonstrate that the new composite wing construction was robust to hydraulic ram. Ballistic tests using armor-piercing (AP) projectiles were conducted at Bell Helicopter Textron Inc. to assess the relative performance of these bonded wings.

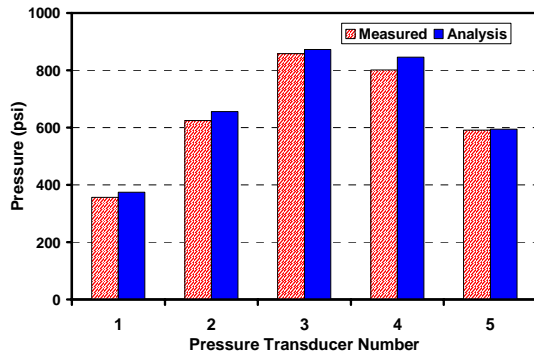


Fig. 13. Comparison of peak pressure at various transducer locations.

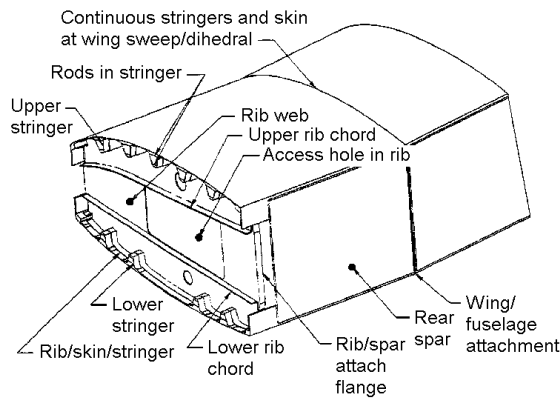


Fig. 14. Composite bonded wing: isometric view.

Each composite wing panel was 41 inches long and 48 inches wide (1.04 m × 1.22 m), with a curved aerodynamic surface representing the upper wing skin. These skin panels were cocured with five stringers and composite ribs bonded to the panels. The panels were individually mounted onto the open side of the aluminum test box to simulate a wing fuel bay of an aircraft. The composite panels with bonded ribs were mechanically fastened to the rib webs and front/rear spar webs of the test box.

A crash-resistant self-sealing fuel cell was installed in the test box before each ballistic test and the fuel cell filled with water, leaving ullage of approximately 10%. Ballistic foam was used to fill the volume between the stringers, support the fuel cell, reduce the probability of dry bay fire, and mitigate hydraulic ram damage to the surrounding structure. Four high-speed pressure transducers were installed on the inside wall of the fuel cell closest to the composite test panels. Two rosette strain gages were mounted to each stringer lower cap; rosette strain gages were also mounted to the outer skin surface directly above the stringer strain gages.

A model of the composite wing used for the simulation is shown in Fig. 15. In this model, the wing structure is connected to adjacent ballistic foam through physical connection at common grids. The ballistic foam and fuel cell wall are connected

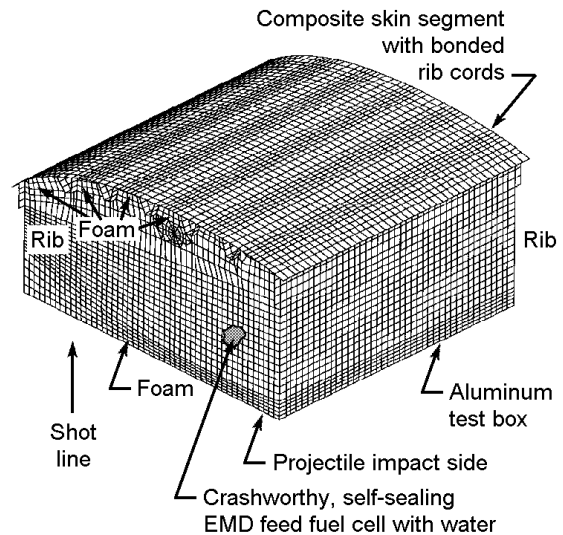


Fig. 15. MSC/DYTRAN model of composite wing test article.

with a rigid connection. The fuel cell wall interacts with fuel through ALE coupling. The interaction between the fuel and projectile is defined using a general coupling. Two adaptive contacts are used to model the interaction between the projectile and entry and exit sides of the wing structure. An adaptive master/slave contact models the interaction of projectile with the fuel cell wall.

The water in the fuel cell is modeled using 51,199 Eulerian hydrodynamic elements. The air in the 10% ullage is also modeled using Eulerian hydrodynamic elements. The Euler mesh is composed of two distinct regions: a central finely meshed region around the shotline and a surrounding region (with mesh gradually becoming coarser) extending to the fuel cell walls. The composite panel representing the upper wing skin in Fig. 15 is modeled with 5,478 composite Lagrangian shell elements with orthotropic material properties. The stringers are modeled with rod elements. The aluminum test box is modeled using 5,428 Lagrangian shell elements representing the 0.160-inch-thick (4.06-mm) aluminum plate. The ballistic foam that fills the space around the fuel cell between the stringers and the aluminum test box is modeled using 4,704 Lagrangian solid elements. The primary purpose of this ballistic foam is to support the fuel cell. The fuel cell wall is modeled using 7,680 Lagrangian shell elements with elastoplastic material properties. The projectile is modeled with 240 Lagrangian shell elements. These elements define the shape of the bullet surface, which for the current simulations is defined as rigid.

The MSC/DYTRAN simulation of the projectile impact at 2,605 ft/s (794.0 m/s) and 0-deg obliquity indicated that the projectile trajectory and the location of the projectile exit (Fig. 16) closely match those observed in the test. The projectile tumbles

slightly as it travels through the fuel cell and impacts the cap on the bottom stringer at the outboard lower area of the skin panel nearly 9 inches (0.23 m) from the rib bond. The projectile exits in the analysis with a velocity of 2,068 ft/s (630.3 m/s), compared with the 1,976 ft/s (602.3 m/s) measured in the test (a 4.7% difference).

Pressure data at two of the four transducers were unreliable. Peak pressures in the Euler elements closest to the two functioning transducers are 172 psi (1,186 kPa) and 750 psi (5,171 kPa). In the ballistic test data, these pressure readings measured 306 psi (2,110 kPa) to 546 psi (3,765 kPa). Only approximate locations for the pressure transducers were available and, due to the finer hydrodynamic mesh in the region of the transducers, there may be a possible discrepancy in the location of the transducers in the Euler mesh. This may explain the difference between measured and computed pressures.

Damage from the ballistic test was limited to one end of the skin panel near the projectile exit location. Simulation indicated that the largest microstrain ($\mu\epsilon$) is 2.625 $\mu\epsilon$ tension and 5.017 $\mu\epsilon$ compression, compared with 1.764 $\mu\epsilon$ tension and 4.241 $\mu\epsilon$ compression measured from the corresponding strain gages in the test. Distortional energy contours from the simulation results, shown in Fig. 17, indicated that limited failure of the stringers is likely.

In the test results, the hydraulic ram pressure delaminated a portion of the forward spar cap. The analysis results of Fig. 18 confirm that the rib flange had high strain levels representative of failure near the forward spar cap.

The high strain contours shown in Fig. 18 correspond closely with the visible bond failure observed in the ballistic test. Strain levels in the analysis are high near the center stringers and along the skin surface between the two lower stringers. Lower strain levels exist in the analysis around the remaining stringers, indicating a good probability of being able to carry load. This agrees with high-

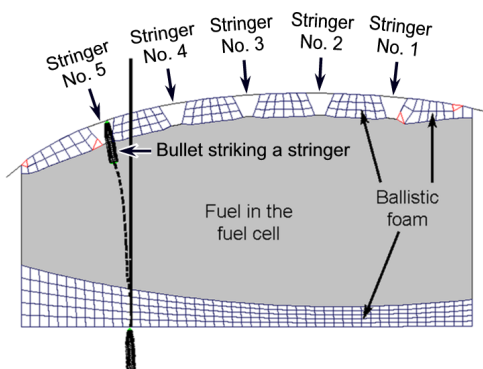


Fig. 16. MSC/DYTRAN model showing projectile exit location for Shot No. 3.

speed film from the test, which indicates that a bondline separation was induced during the test, but did not propagate substantially.

As in the case of the generic tank, the physics of ballistic dynamics phenomenon are closely replicated for the composite wing tank. Thus MSC/DYTRAN has the potential of being a useful design tool for enhancing ballistic tolerance.

Based on the ballistic simulations conducted herein, MSC/DYTRAN appears to be a promising tool for improving ballistic tolerant designs and in guiding pretest line-of-shot setup. MSC/DYTRAN can be used to directly simulate the full sequence of hydraulic ram and can be effectively used to predict projectile trajectories and tumbling behavior.

Crash Analysis of an Energy-Absorbing Subfloor in a Hard Surface Impact

During hard surface impacts, concentrated loads are introduced into the stiffest structural members, such as keel beams and frames. As a number of crash impacts occur on hard surfaces, the energy-absorption behavior of subfloor concepts during hard surface impacts needs evaluation. This problem focuses on the vertical drop simulation of an airframe subfloor design for a hard surface impact 24 ft/s (7.3 m/s) and its comparison with the test data. The resulting analytical results such as peak acceleration pulse, duration, and onset rates at

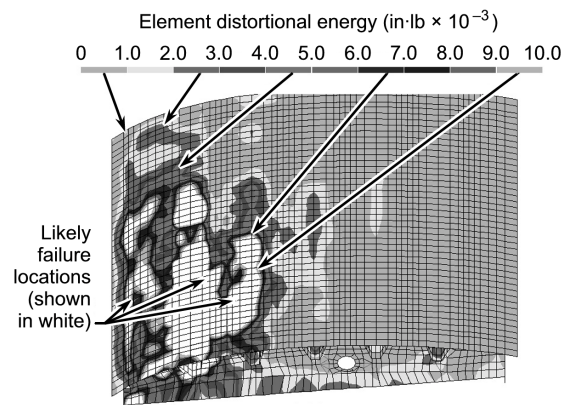


Fig. 17. Failure locations from Shot No. 3 ballistic simulation.

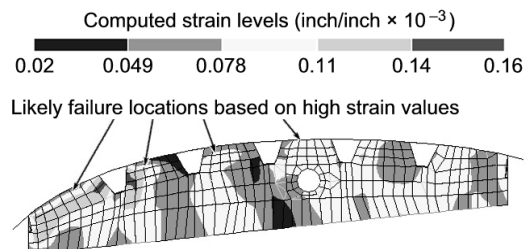


Fig. 18. Strain contours on the wing rib for Shot No. 3.

the seat location were compared with measured test data available from Ref. 10.

Description of Subfloor Structure

The concept was designed for airframe strength, stiffness, and crash-energy absorption. The design had to be practical relative to cost and producibility, as well as allow normal routing of controls, wiring, and plumbing.

The test section was 48 inches wide and 42 inches long (1.22 m × 1.07 m). The maximum floor depth of the combined floor and the bulkheads constituting the crush zone was 8.0 inches (0.20 m). A strong floor in the top 2.0 inches (5.08 cm) was designed to transmit the seat and airframe loads into the EA subfloor structure while maintaining structural integrity for seat retention and occupant protection. With the exception of the seat tracks, which were constructed from 7075 aluminum, the material used in the test specimen was 2024-T3 aluminum alloy.

The subfloor section consisted of double 6.0-inch diameter (15.24 cm) cylinders that functioned as keel beams (Fig. 19) running between the 0.032-inch-thick (0.0812-cm) aluminum belly skin and floor structure. The belly was flat with no curvature inboard of BL 11.5. Lateral ring frames fabricated from 0.025-inch-thick (0.0635-cm) aluminum supported the keel cylinders. Each longitudinally extending cylinder was 6 inches (15.24 cm) in diameter and made from 2024-T3 aluminum, 0.020 inch thick (0.0508 cm). During the hard surface impacts, the two cylinders were filled with rigid PVC foam of 1.5 lb/ft³ (16.01 kg/m³) density.

Two loading platforms representing conventional seats were ballasted with two lumped masses that weighed 165 lb (74.84 kg), to simulate two occupants. The loading platform frames attached to longitudinally running seat tracks with standard seat interface hardware. With the test section alone weighing 39.0 lb (17.69 kg, including 2.0 lb [0.91 kg] of foam), the total test fixture weighed 435 lb (197.3 kg).

Hard Surface Impact Test

In the dynamic test, the subfloor impacted a hard surface at 24 ft/s (7.31 m/s). The post-test subfloor structure is shown in Fig. 20, and the corresponding analysis model is shown in Fig. 21. Acceleration data were measured at the seat mass and at the base of the seat frame on the floor. Only the left seat and floor data were available. While the acceleration data are not digitally filtered, they were recorded with a 600-Hz low-pass filter in the recording system and digitized at 4,000 samples/second.

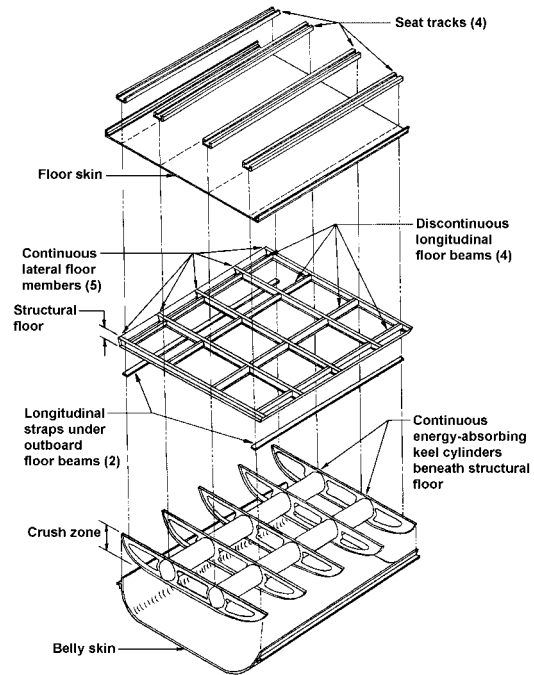


Fig. 19. Exploded view of subfloor structure.

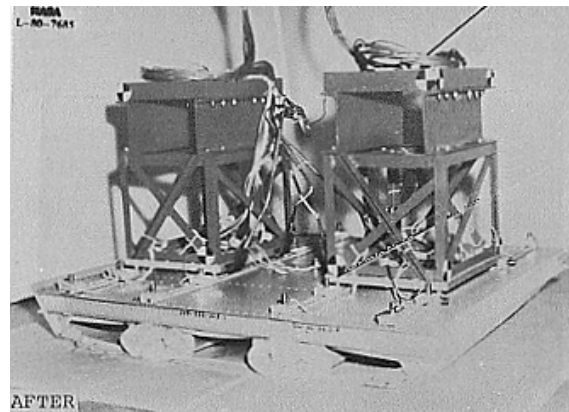


Fig. 20. Subfloor after hard surface impact.

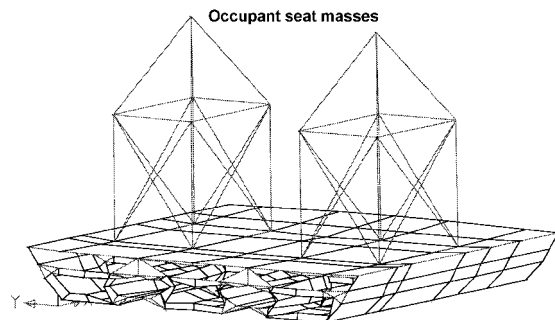


Fig. 21. Coarse subfloor model after hard surface impact analysis.

The measured accelerometer data at the left seat lumped mass (Fig. 22) indicate that the subfloor provided a relatively constant 40g pulse for about 0.034 second with a peak acceleration of 47g. The floor deceleration shows that the floor crushed at the same load, but low-amplitude higher frequency floor vibrations are superimposed. No documentation exists in Ref. 10 quantifying the amount of subfloor deformation, but visual observation (as well as double integration of the acceleration data) suggests a residual crush of approximately 3 inches.

Analysis of Hard Surface Impact

An MSC/DYTRAN model of this subfloor structure (Fig. 21) was analyzed for a 24 ft/s (7.31 m/s) impact on a rigid surface. A surface-to-surface contact allowed force-interaction of subfloor belly skin with the ground. The model is termed “Coarse Straight,” since it was relatively coarse and lacked explicit modeling of crush initiators on the bulkhead-to-belly-skin transition. This model used 503 nodes, 174 bar elements, 386 quadrilateral shells with Belytschko-Tsay formulation, and 190 triangular shell elements with a co-triangle formulation. These elements, all composed of 2024-T3 aluminum, represented five bulkheads and lateral floor members, and four discontinuous longitudinal beams on which inboard and outboard seat tracks are mounted, floor and belly skin as well as the seat structure. An elastoplastic stress-strain curve and maximum plastic strain-to-failure criteria constituted the material model used in the analysis. To keep the model simple, the larger flange radius at the notched corners (angles) for attaching the bulkheads to the sub-floor was not modeled, which resulted in a higher initial pulse. The subfloor belly was covered with 96 faces to model the surface required for sub-floor belly-to-ground contact force interaction. In addition, a single surface contact was modeled for the whole subfloor structure to account for floor crush on bulkheads and belly skin as well as for the bulkhead crush onto itself or belly skin.

The coarse subfloor model after the hard surface impact simulation is shown in Fig. 21. Because of the symmetry in the analysis model, the right and left seat accelerations are identical. The resulting acceleration computed at one of the seats for the hard surface impact averaged around 40g and reached a peak of approximately 47g, as shown in Fig. 22. The total pulse duration of 0.034 second compared very favorably with the test data. As in the test, the analysis data were low pass filtered at 600 Hz frequency. A higher initial acceleration peak was experienced between analysis time (t) of 0.001 and 0.002 second, due to the lack of crush radius from bulkheads to belly skin. Without this crush radius, the bulkheads (which constitute the primary

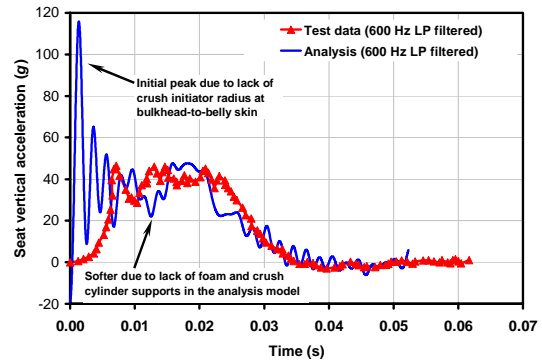


Fig. 22. Computed seat vertical acceleration for coarse model in hard surface impact analysis.

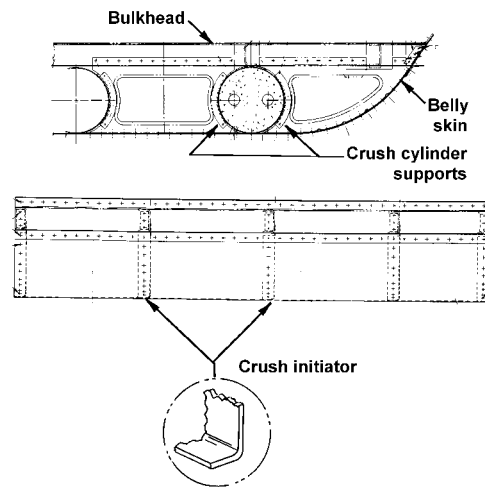


Fig. 23. Crush cylinder support and crush radius details.

crush zone) have to overcome the buckling load. Around $t = 0.01$ second, the computed acceleration shows a dip compared with test data. This may be due to the lack of modeling the foam and the four 6.0- × 2.0-inch (15.24- × 5.08-cm) strips of 0.0250-inch (0.0635-cm) thick supports, two on either side of crush cylinder (Fig. 23) on each bulkhead. Since crush cylinders are the first to strain, the overall model acts softer than the real structure. Other than this discrepancy, the coarse model with straight bulkhead-to-skin transition accurately simulates the acceleration pulse. The foam was not modeled because foam properties were not available at that time in a format that could be characterized by one of the available materials in MSC/DYTRAN.

Peak deformation at the seat as well as the floor was approximately 2.6 inches (6.35 cm). This is in general agreement with visual observations from Fig. 20. The floor acceleration pulse-peak and duration were comparable to the test data and showed significantly more ringing compared with the seat acceleration pulse.

Effect of Refined Structural Mesh Density

To determine the effect of refined structural modeling on analytically predicted hard surface impact response, a detailed subfloor model was developed with straight bulkhead-to-skin transition. This model, termed “Detailed Straight,” was composed of 14,898 grids, 15,082 quadrilateral shell elements, 130 triangular shell elements, and 386 bar elements, as shown in Fig. 24. Since the detailed model was developed concurrently with the coarse model, the foam and crush cylinder supports (Fig. 23) were not included at that time. The effect of this Lagrangian mesh refinement on hard surface impact response at the seat locations is shown in Fig. 25. All analysis data is low pass filtered at 600 Hz to correspond with test data for hard surface impact. The acceleration pulse for the “Detailed Straight” model shows duration of 0.035 second with a peak of 49g, ignoring the first peak caused by the lack of crush radius. Refined modeling helps attenuate the initial acceleration peak; however, the overall pulse shape does not show much improvement from the “Coarse Straight” model. Modeling the crush radius for the detailed model attenuates the initial peak even further, as shown by the “Detailed Canted” line in Fig. 25.

To summarize, subfloor structures undergoing hard surface impacts can be analyzed using MSC/DYTRAN fairly accurately using relatively coarse finite-element models. Use of a piecewise linear material stress-strain model, a yield model, and a failure model results in accurate acceleration pulse peaks, duration, and shape. However, modeling of a crush initiator radius, and possibly foam, is necessary to simulate accurate initial acceleration pulse.

Rotorcraft Water Ditching

In this section, the MSC/DYTRAN code was used for analysis-test correlation of aircraft during calm water ditching. Crash-resistant features built into rotorcraft components, as well as crash criteria such as MIL-STD-1290, and design methodologies such as Aircraft Crash Survival Design Guide, are based on hard surface impacts. Accident data, however, indicate that only 18% of potentially survivable civilian crashes occur on hard, prepared surfaces (Ref. 11). The statistics are even lower for the Army at 7% and the Navy at zero percent. In contrast, 51% of civilian and 83% of Navy crashes occur on water and soft soil.

The crash-resistant subsystems designed for rigid surface impacts, such as landing gear or subfloors, are not as effective in water and soft soil, since the structure undergoes a different loading

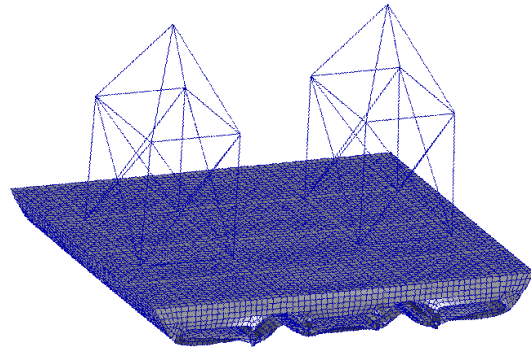


Fig. 24. Detailed subfloor model after hard surface impact analysis.

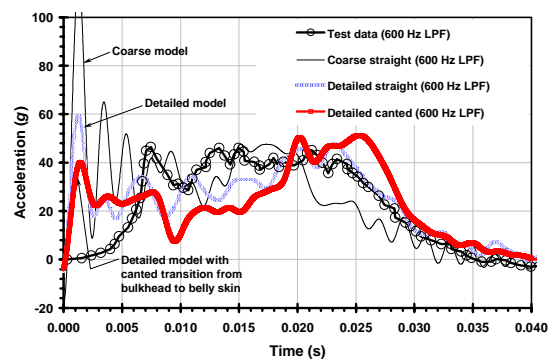


Fig. 25. Effect of refined mesh density and crush radius on seat vertical acceleration in hard surface impact analysis.



Concentrated loading
(hard surface impacts)

Distributed loading
(water/soft soil impacts)

Fig. 26. Loading mechanism for hard surface and water/soft soil impact.

mechanism. Whereas hard surface impacts introduce concentrated loads into the stiffest subfloor structural members, such as keel beams and frames, water and soft soil impacts introduce distributed crash loads across the belly skins in a highly rate-sensitive manner, as illustrated in Fig. 26. If the structural integrity of the belly skins can be maintained during a water impact, the crushable energy-absorbing keel beams can be used to control the loads introduced into the airframe. Additional energy absorption may also be provided by deformation of the subfloor surface.

Since most crash impacts occur on soft soil or water, the energy-absorption behavior of structures during water impacts should also be better understood. Accordingly, an MSC/DYTRAN-based water crash dynamics methodology (Ref. 7 and 8) has been under development to predict rotorcraft crash performance during water impacts. The methodology allows evaluation of surface pressures, skin rupture, and subfloor and seat acceleration levels, as well as evaluation of energy absorption by the airframe subfloor.

Before assessing water impact methodology for practical airframe structures, Bell evaluated the water-impact of a 10-degree deadrise angle wedge. Data from the corresponding water-impact tests (conducted at David Taylor Model Basin) were used for correlation. Once the water-impact models correlated well with the test data, full-fuselage water-impact models were constructed.

The next step in methodology development involved analysis–test correlation for tiltrotor scale model during calm water ditching at 6 ft/s (1.8 m/s) sink rate and a forward speed of 30 kn (55.56 km/h) (Ref. 7). Since water impact test data were available for a scale model of a tiltrotor at 42,600 lb (1.932 kg) GW (Fig. 27), this configuration was selected for water impact analysis under calm sea conditions. The fuselage of the aircraft was modeled with MSC/DYTRAN using 2,977 rigid planar elements as shown in Fig. 28. The wing and nacelles were not represented, since test data indicated the peak pressures and accelerations occurred while the aircraft is still in a nose-up pitched attitude and thus prior to water contact with the nacelles. However, efforts subsequent to completion of this work have included deformable subfloor structure as well as wing and nacelles structures.

Although fluid modeling using Lagrangian solids with no yield strength was attempted, the contour mapping of fuselage underside pressures is currently available only for Eulerian meshes. Therefore, subsequent modeling used 32,400 Eulerian elements to represent the water and 10,800 Eulerian elements to model the air above the water mesh. The total Eulerian mesh covered an area of 1,200 inches long by 600 inches wide and 100 inches deep (30.48 m × 15.24 × 2.54 m). The fluid mesh in the area of initial impact had elements each with a size of 13 inches long by 13 inches wide and 10 inches deep (33.02 cm × 33.02 cm × 25.4 cm). The Eulerian air mesh height of 3 ft (0.9144 m) above the water surface was used to maintain general coupling between the Lagrangian fuselage and the Eulerian water after rebound and secondary recontact.

Using the Eulerian fluid mesh, the MSC/DYTRAN analysis results at 30 kn (55.56 km/h) forward velocity, 6 ft/s (1.82 m/s) sink rate, 67% rotor lift, and 10-deg nose-up attitude condition



Fig. 27. Scale model water impact test.

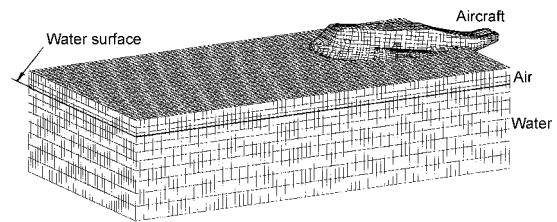


Fig. 28. MSC/DYTRAN model of aircraft and fluid.

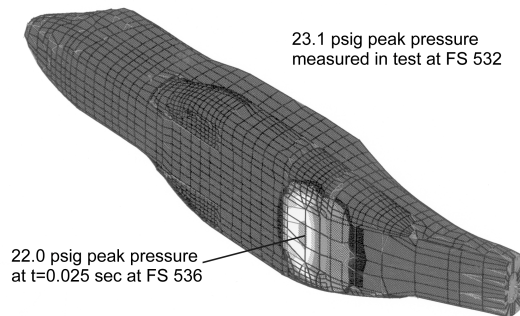


Fig. 29. Impact pressure for ditching for 30 kn forward velocity and 6 ft/s sink rate.

show the aircraft reaching a nearly level attitude at approximately 0.50 seconds, consistent with the reported test results. Initial impact at 0.005 seconds resulted in a peak pressure of 21.0 psig (1.0 kPa) at fuselage station (FS) 550. At 0.025 seconds, a peak fluid pressure of 22.0 psig (1.05 kPa) is noted in the analysis at FS 535.5 as shown in Fig. 29 (versus approximately 23.1 psig (1.11 kPa) measured in test at FS 532). Thereafter, the peak fluid pressure continues to decline to approximately 4 to 6 psig (0.191 to 0.287 kPa) as the aircraft levels off.

At the aircraft cg, the analysis indicates a peak vertical deceleration of 2.5g was reached as shown in Fig. 30 (versus test results of 1.9g at FS 412 near the cg). Correspondingly, the longitudinal deceleration peaks at 0.35g as shown in Fig. 30 (versus 0.7g measured in test). The corresponding reduction in vertical and longitudinal velocity at the fuselage cg is shown in Fig. 31. As the aircraft sinks into the

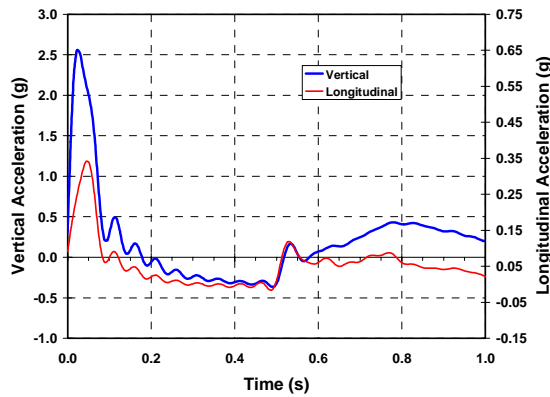


Fig. 30. Acceleration time history at fuselage cg for 30 kn forward velocity and 6 ft/s sink rate.

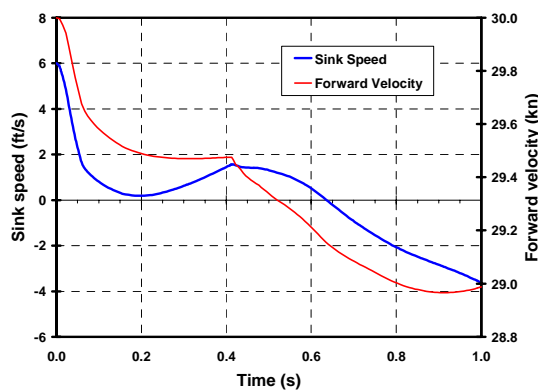


Fig. 31. Aircraft cg velocity time history for 30 kn forward velocity and 6 ft/s sink rate.

water and drags forward, the nosedown (negative) pitching moment of the aircraft cg continues to increase until the aircraft starts to level off and areas ahead of FS 550 and longitudinally closer to the aircraft cg impact the water at approximately 0.50 seconds.

To improve the acceleration correlation, subsequent efforts have focused on investigation of modeling parameters and techniques. Furthermore, airframe flexure is being added into the current full fuselage MSC/DYTRAN models to assess the effect of flexibility on reducing skin pressures and airframe accelerations.

To summarize, the analysis described in this section indicates that MSC/DYTRAN can be used to effectively simulate airframe water ditching.

Bird Strike Analysis of Airframe Structure

Another example is the use of MSC/DYTRAN to determine design loads for a 4.0-lb (1.8-kg) bird impacting the wing leading edge and horizontal stabilizer of the BA609 at 240 kn (445 km/h). The

analysis model for this work contains two primary components: an Eulerian bird model using consistent mass representation and a Lagrangian leading edge. The analysis simulation shows that deformation of the leading edge plays a significant role in momentum transferred to the supporting structure.

Fig. 32 shows both the analytical MSC/DYTRAN model of wing leading edge being impacted by a 4-lb (1.8 kg) bird as well as the corresponding impact of the bird during wing leading edge bird-strike tolerance test. A methodology was developed to analyze both metallic and composite wing leading edge configurations. For metallic wing leading edges, two leading edge configurations of different gauge thickness, each of 7075-T6 aluminum, 2024-T3 aluminum, and a 6AL-4V titanium alloy were tested and analyzed with excellent comparison of results. For metallic leading edges, the analysis models used material characterization in elastoplastic formulation while for composite leading edges, detailed ply orientation, thickness and material strength data in various directions along with the failure and post-failure degradation model were used. The success of the results was based mainly on predictions of maximum wing leading edge displacement towards the wing spar web. As such, these MSC/DYTRAN-based analytical simulations are very useful for providing test guidance as well as reducing the number of expensive tests.

Concluding Remarks

This paper summarizes the results of applications of a nonlinear dynamics tool, MSC/DYTRAN, to a number of important design support problems involving material and geometric nonlinearity as well as structure-to-structure and/or fluid-structure interaction. The paper demonstrates that this commercially available nonlinear dynamics software code is a viable design tool for simulating skid gear dynamic drops, ballistic impacts, rotorcraft water ditching, subfloor hard surface impacts, and bird strike tolerance.

Acknowledgments

Portions of this paper are based on materials previously published in the *Proceedings* of the American Helicopter Society Annual Forum, and are used by permission.

References

1. Sareen, A. K., Smith, M. R., and Howard, J. V., "Helicopter Skid Gear Dynamic Drop Analysis and Test Correlation," *Proceedings of the American Helicopter Society 54th Annual Forum*, Washington, D.C., May 20–22, 1998.

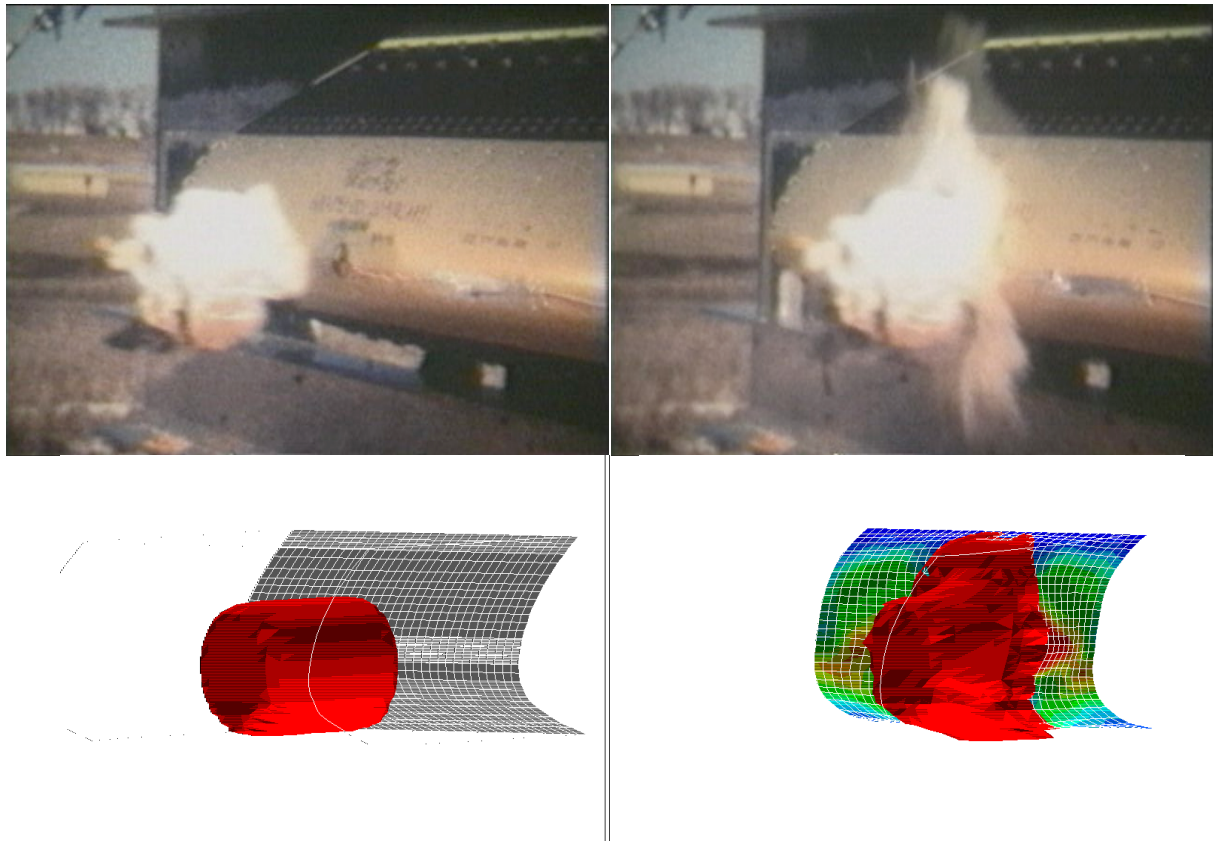


Fig. 32. Simulation of a wing leading-edge bird strike test using MSC/DYTRAN.

2. Stephens, B. E., and Evans III, W. L., "Application of Skid Landing Gear Dynamic Drop Analysis," Proceedings of the American Helicopter Society 55th Annual Forum, Montreal, Quebec, Canada, May 25-27, 1999.
3. Sareen, A. K., and Smith, M. R., "Evaluation of an Analytical Design Tool for Ballistic Dynamics Simulation," Proceedings of the American Helicopter Society 52nd Annual Forum, Washington, D.C., June 4-6, 1996.
4. Sareen, A. K., and Smith, M. R., "Evaluation of an Analytical Design Tool for Ballistic Dynamics Simulation," Proceedings of the 1996 MSC World User's Conference, Newport Beach, CA, June 3-7, 1996.
5. *Crash Simulations of Energy-Absorbing Single Cruciform Crashworthy Helicopter Subfloor Structure*, Bell Helicopter Textron Inc. Subcontractor Final Report to Simula Government Products Inc. under contract DAAJ02-93-C-0030, December 10, 1996.
6. *Composite Structure Damage Assessment: A Proposal Concept*, Transmotive Technologies, Inc., Report No. TM 97-06-185, June 17, 1997.
7. Wittlin, G., Smith, M. R., Sareen, A. K., and Richards, M., "Airframe Water Impact Analysis Using a Combined MSC/DYTRAN-DRI/KRASH Approach," Coauthor, Proceedings of the American Helicopter Society 53rd Annual Forum, Virginia Beach, VA, April 29-May 1, 1997.
8. *Water Crash Dynamics and Structural Concepts for Naval Helicopters*, Bell Helicopter Textron Inc. Subcontractor Final Report to Dynamic Response Inc. under contract N62269-96-C-0044, September 1996.
9. "Aeronautical Requirements-Structural Design Requirements - Helicopters," AR-56, Naval Air Systems Command, Department of the Navy, 1970.
10. Cronkhite, J. D., and Berry, V. L., *Crashworthy Airframe Design Concepts*, NASA CR-3603, September 1982.
11. Sareen, A. K., Smith, M. R., and Hashish, E., "Crash Analysis of an Energy-Absorbing Subfloor during Ground and Water Impacts," Proceedings of the American Helicopter Society 55th Annual Forum, Washington, D.C., May 25-27, 1999.



Clearance and Copyright Form

Title of paper: APPLICATIONS OF A NONLINEAR DYNAMICS TOOL TO ROTORCRAFT
DESIGN PROBLEMS AT BELL HELICOPTER TEXTRON

Name(s) of author(s): ASHISH K. SAREEN, MICHAEL R. SMITH, B. ROBERT MULLINS

Clearance

This paper is UNCLASSIFIED (for public release) and has been cleared by the appropriate agencies – company and government. I understand that no corrections can be made after the paper has been sent to the ERF secretariat.

Signature of Author(s):

Ashish K. Sareen; B. Robert Mullins
Michael R. Smith

Date:

6/30/2001

Non-infringement statement

This paper represents original work by the authors(s). No portion of the material is covered by a prior copyright; or for any portion copyrighted, the author has obtained permission for its use.

Signature of Author(s):

Ashish K. Sareen; B. Robert Mullins
Michael R. Smith

Date:

6/30/2001

Copyright release

KAMOV Company holds the copyright of the paper, with the clear understanding that I (as the author) and the author's organization have the right to reproduce it for their own purposes, in part or in full, provided they are not for sale, and the right to use, free of charge, all or portions of the above paper in future works of their own, such as books and lectures. The copyright notice will read: Copyright 2001 by KAMOV Company.

Signature of Author(s):

Ashish K. Sareen; B. Robert Mullins
Michael R. Smith

Date:

6/30/2001

Publication on electronic media

I agree with the publication of the abstract of my paper on the Internet and I agree with the publication of my paper on a CD-ROM, published by the 27th ERF Organization Committee and distributed without royalties to the authors.

Signature of Author(s):

Ashish K. Sareen; B. Robert Mullins
Michael R. Smith

Date:

6/30/2001

Please fill in and return this form before June 15 to the Forum Secretariat:

European Rotorcraft Forum Secretariat
KAMOV Company
Attn: Mrs. V. Popova
8A, March 8th Street
140007 Lubertsy RUSSIA

Tel/Fax: 7-095-554-3256
Tel/Fax: 7-095-700-3071
E-mail: erf2001@kamov.ru
Web site: www.kamov.ru